Young's double-slit interference for quantum particles

Zehra Nur Ozer,[1] Hari Chaluvadi,[3] Melike Ulu,[1] Mevlut Dogan,[1] Bekir Aktas,[2] and Don Madison[3]
[1]*Department of Physics, e-COL Laboratory, Afyon Kocatepe University, 03200, Afyonkarahisar, Turkey*
[2]*Department of Physics, Gebze High Technology Institute, Gebze, Turkey*
[3]*Department of Physics, Missouri University of Science and Technology, Rolla, Missouri, USA*
(Received 4 January 2013; revised manuscript received 12 March 2013; published 16 April 2013)

For the last 50 years, there has been considerable interest in the possibility of observing the equivalence of a Young's double-slit wave interference at the quantum level for diatomic molecules. For electron-impact ionization of diatomic molecules, indirect evidence for this type of interference has been found by changing the energy (wavelength) of the ejected electron while keeping the incident projectile scattering angle fixed. The present work represents an experimental and theoretical collaboration to better understand the physics of this type of interference. In addition to examining the effect of changing the ejected electron energy for a fixed scattered projectile angle, we have also examined the effect of keeping the ejected electron energy fixed while varying the projectile scattering angle. Model calculations are performed for three different types of possible two-center interference effects, and it is found that the most important one is diffraction of the projectile off two scattering centers.

DOI: 10.1103/PhysRevA.87.042704 PACS number(s): 03.65.Nk, 34.80.Dp, 34.80.Gs

I. INTRODUCTION

In the famous Young's double-slit experiment, the wave nature of light was demonstrated by observing the constructive and destructive interference pattern resulting from two light waves emitted from two closely spaced slits. In 1966 Cohen and Fano [1] suggested a quantum-mechanical equivalent in which light incident on the double slits is replaced by light incident on and ionizing a diatomic molecule. Cohen and Fano [1] considered the two atoms in the molecule as independent absorbers of light which then became two separate sources for the emission of photoelectrons which would then produce an interference pattern. Due to particle-wave duality, similar interference effects should be expected if the incident light is replaced by particles and in 2001, Stolterfoht *et al.* [2] reported evidence for interference effects for Kr^{34+} ionizing H_2 in which the ejected electrons were detected but the scattered projectiles were not. These cross-section measurements were doubly differential in the energy and angle of the ejected electron so we will label them DDCS(electron). In the Cohen and Fano [1] model where the interference arises from electron waves being emitted from two different centers, one would expect that the important parameter would be how the wavelength of the emitted electron compared to the slit separation (i.e., internuclear distance) so measurements were performed as a function of the electron energy (i.e., wavelength).

Since the first DDCS(electron) measurements were reported for heavy particle impact, there have been a large number of papers published for different heavy projectiles and different energy ranges [3–9]. However, all these measurements were performed as a function of the ejected electron energy. More recently, Alexander *et al.* [10] measured cross sections for 75-keV proton impact ionization of H_2. They performed a DDCS(projectile) measurement where the energy and angle of the scattered proton is measured instead of the ejected electron. They showed that the interference effects were more sensitive to the angular dependence of the scattered projectile than to the energy dependence of the ejected electron. Egodapitiya *et al.* [11] showed that, for heavy particles, one can control the perpendicular width of the projectile wave packet such that either both scattering centers are exposed to the beam (H_2 scattering) or only one scattering center is exposed (H scattering), and interference effects are seen when both centers are exposed and no interference is seen when only one center is exposed. Using this technique, Sharma *et al.* [12] showed that one can simultaneously measure cross sections for atomic hydrogen and molecular hydrogen and get the interference effects in a single measurement without relying on any theoretical calculations or second independent experiment.

Electrons as projectiles should be better than heavy particles for investigating interference effects since they have larger de Broglie wavelengths for identical velocities and are more easily deflected. Also, it is much easier to measure fully differential cross sections [normally called triply differential cross sections (TDCS)], which should be more sensitive to interference than DDCS measurements. For TDCS measurements, the energy and angular location of both final-state electrons are simultaneously determined. Murray *et al.* [13] were the first to look for interference effects in low-energy TDCS measurements for electron-impact ionization of H_2 and they found no evidence for interference.

Cohen and Fano [1] pointed out that since the measured cross sections typically fall by orders of magnitude as a function of electron energy, the interference effects can be seen more readily by taking a ratio of the molecular cross section to the corresponding atomic cross sections. This ratio is called the interference factor (I), and the idea is that the cross section for a diatomic molecule should be equal to the atomic cross section times the interference factor, which should be an oscillating function that exhibits the constructive and destructive interference effects. Stia *et al.* [14] examined the interference factor for electron-impact ionization of H_2, and they found that the TDCS interference factor for electron-impact ionization could be approximated the same as Cohen and Fano [1] found for photoionization:

$$I^{CF} = \frac{\sigma_{H_2}}{2\,\sigma_H} = 1 + \frac{\sin(QD)}{QD}. \quad (1)$$

Here $\mathbf{Q} = \mathbf{k}_0 - \mathbf{k}_a - \mathbf{k}_b$ is the momentum transferred to the residual (recoil) ion, $\mathbf{k}_0, \mathbf{k}_a$, and $\mathbf{k}_b$ are the momentum of the incident, scattered and ejected electrons, respectively, and D is the equilibrium internuclear distance in the target molecule (1.4 a.u. for H_2). All molecular orientations have been averaged in the evaluation of Eq. (1).

Typical $(e,2e)$ TDCS measurements plotted as a function of the ejected electron angle for a fixed projectile scattering angle exhibit a large peak for small ejection angles and a smaller peak for large ejection angles. (Although we do not know which electron is the projectile and which one is ejected, for discussion purposes we will refer to the faster final-state electron as the scattered projectile and the slower electron as the ejected electron.) The small-angle peak is called the binary peak, since it is normally close to the classical billiard ball angle for a collision between the incident electron and an electron at rest. The large-angle peak is called the recoil peak and it is attributed to electrons backscattered from the nucleus. Depending on the kinematics, the interference factor of Eq. (1) predicts that the molecular recoil peak should be either suppressed or enhanced relative to the atomic one.

Milne-Brownlie *et al.* [15] measured TDCS for 250-eV electron-impact ionization of H_2 and three different ejected electron energies. For the kinematics of their experiment, Eq. (1) predicts that the recoil peak for H_2 should be suppressed relative to the atomic cross section and this was verified by their experiment. Milne-Brownlie *et al.* [15] just looked at the relative sizes of the binary and recoil peaks and not directly at the interference factor I. Next Casagrande *et al.* [16] performed a similar experiment for higher energies ($\sim$600 eV) and they looked directly at the experimental interference factor of Eq. (1), which predicted suppression of the recoil peak for some energies and enhancement for other energies, and they found good agreement with I^{CF}.

Consequently, the current situation for electron-impact TDCS is that existing measurements of the interference parameter I are in good agreement with I^{CF}, which is based upon the assumption that the two atoms in the molecule are independent absorbers of energy which then became two separate sources for the emission of electrons which then produce an interference pattern.

Both of the TDCS studies reported so far were performed for an ejected electron energy scan for a fixed projectile scattering angle similar to the DDCS(electron) studies for heavy projectiles. As mentioned above, Alexander *et al.* [10] showed from DDCS(projectile) measurements that interference effects were more sensitive to scanning the projectile scattering angle than to scanning the ejected electron energy for proton collisions. In the Cohen-Fano model, the incident projectile (or light) is just a source of energy which is transferred to the atoms, causing them to become an electron emitter, and one would expect a weak dependence on the projectile scattering angle and a strong dependence on the ejected electron wavelength. If the projectile scattering angle is more important than the ejected electron energy, the current model of interference resulting from electron waves emitted from two centers would come into question.

Here we report a study of the interference factor I for 250-eV electron-impact ionization for both an energy scan with a fixed projectile angle and a projectile angle scan with a fixed ejected electron energy. We find that the interference factor (1) has significantly more structure than predicted by I^{CF} and (2) there is a stronger dependence on projectile scattering angle than on ejected electron energy. These results indicate that the current model is incomplete and that additional two-center effects are important for these energies. We investigate three possible two-center effects: (1) an incident electron diffracted by two scattering centers; (2) a scattered projectile in the field of two scattering centers; and (3) an ejected electron in the field of two scattering centers. We find that the most important double-slit effect is the incident electron diffracted by two scattering centers.

To validate our experimental results, we chose the same kinematics as Milne-Brownlie *et al.* [15] for the energy scan and we followed the same procedure as both Milne-Brownlie *et al.* [15] and Casagrande *et al.* [16], who compared the molecular H_2 results to atomic He instead of atomic H. From an experimental point of view, using He is obviously desirable due to the difficulty of measuring atomic H cross sections. However, the implicit assumption is that single-center scattering effects are the same for both H and He such that the interference factor ratio contains only double-scattering effects. To our knowledge, this assumption has never been checked. Our results provide some indirect evidence for the validity of this assumption.

II. EXPERIMENTAL APPARATUS AND PROCEDURE

This apparatus has been used before in several experiments [17–20] by Albert Crowe's group in Newcastle. The experimental apparatus, acquired from a UK grant, was moved to Afyon Kocatepe University, Turkey, in 2007 and is now used in electron-electron coincidence experiments. The experimental setup and procedure are in principle identical to those used by Sise *et al.* [21]. The description of the apparatus can be divided into (a) the implementation of the general principles of the electron spectrometer with special features for the electronic detection and (b) the data acquisition systems. The electron spectrometer consists of an electron gun, two hemispherical analyzers, and a Faraday cup. All these components are housed in a vacuum chamber with a base pressure of $\approx 8 \times 10^{-8}$ mbar. The spectrometer is kept in the vacuum chamber with μ-metal shielding, which reduces the surrounding magnetic fields in addition to the Helmholtz coils.

Figure 1(a) shows a schematic representation of the present experimental apparatus. The energy of the electron beam could be varied between 40 and 350 eV, with an energy width resolution less than 0.6 eV. The typical electron-beam currents used in these experiments ranged from 3 to 5 μA, as detected on the Faraday cup.

The electron beam was crossed perpendicularly with a gas beam, formed by a nozzle with 2 mm diameter. In a well-defined electric field configuration, the electrons are projected onto the electron analyzers. The two electron analyzers are located on separate turntables inside the vacuum chamber which can rotate around the detection plane. The effective angular range is limited by the presence of the Faraday cup in forward angles and the electron gun in the backward angles. To reduce the angular limitations, a small Faraday cup is

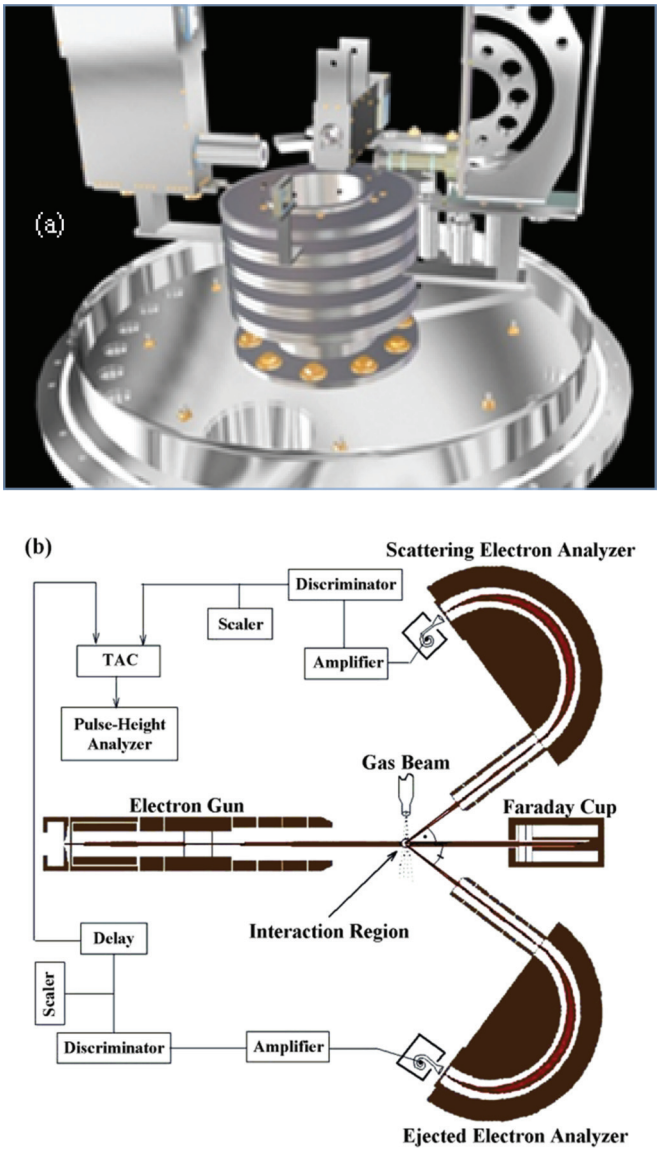

FIG. 1. (Color online) Sketch of electron spectrometer. The main components are (a) electron gun, two electron analyzers, and Faraday cup; and (b) coincidence electronics used to accumulate the coincidence timing spectrum at each set of kinematics.

placed onto the large Faraday cup, which allows us to measure scattering angles down to 35 degrees.

The method used for computerized data collection and analysis has also been described in detail in [21,22]. The electron beam is produced by the electron gun via a filament crossed with the gas. The two outgoing electrons are detected using hemispherical electron analyzers with channel electron multipliers (CEMs) [Fig. 1(b)]. The signals acquired from the CEMs are processed via amplifier and discriminator circuits. The two time-correlated electrons are detected in coincidence. The output pulses from the coincidence electronics are recorded via a Trump-PCI interface card as a time spectrum which contains the true coincidence signal. Results were recorded by computer software (Maestro) and saved before the analyzer is rotated to another angle. The true coincidence count rate was determined in an usual way, from the difference

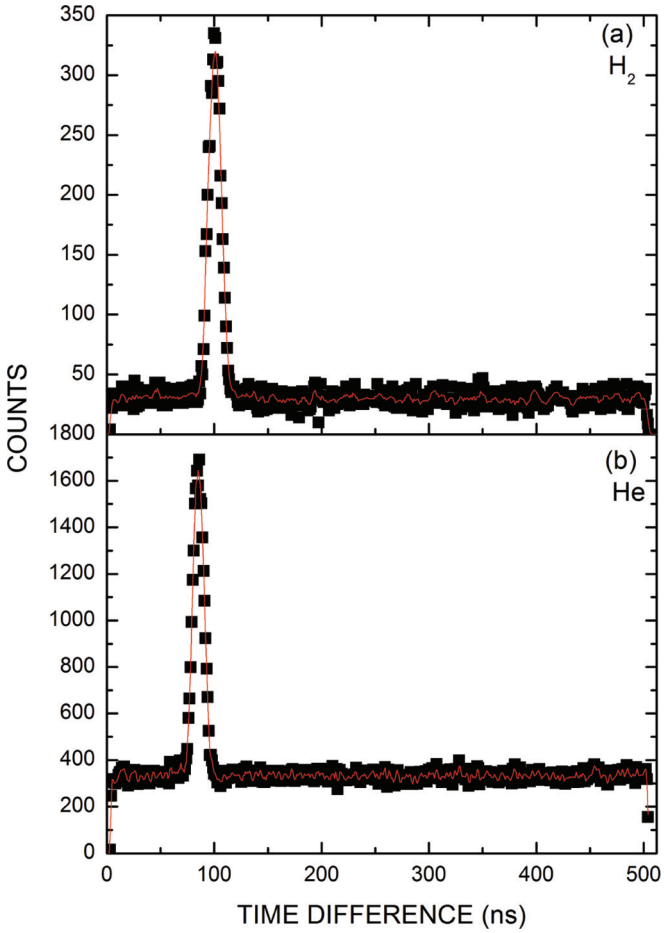

FIG. 2. (Color online) Typical coincidence peaks for H_2 (a) and He (b) for $E_0 = 250$ eV, $E_b = 50$ eV, and $\Theta_a = -15^\circ$.

between true-plus-random and random coincidence rates. The statistical accuracy of the true coincidence data was determined by the uncertainty in the measurement of both the true and random coincidence counts. The interaction region must be precisely positioned at the center of the rotation of the analyzers and the electron gun (50 mm away from the interaction region).

To establish the kinematics for the measurement, the incident and ejected electron energies were chosen and the scattered electron energy was determined by energy conservation:

$$E_0 = E_a + E_b + V_I. \tag{2}$$

Here (E_0, E_a, E_b) are the incident, scattered, and the ejected electron energies, respectively, and V_I is the ionization potential (24.6 eV for He and 15.4 eV for H_2).

Measurements in the study were obtained using an asymmetric coplanar geometry. In this geometry, the two outgoing and the incident electrons are all in the same plane. Figure 2 shows a coincidence peak obtained for H_2 and He for the same kinematics. The width of the coincidence peak at half maximum (FWHM), under the same conditions for both targets, is approximately 12 ns.

The uniform background in the coincidence spectra is caused by the arrival of fully uncorrelated electrons in the detectors. The peak that is superimposed on these background

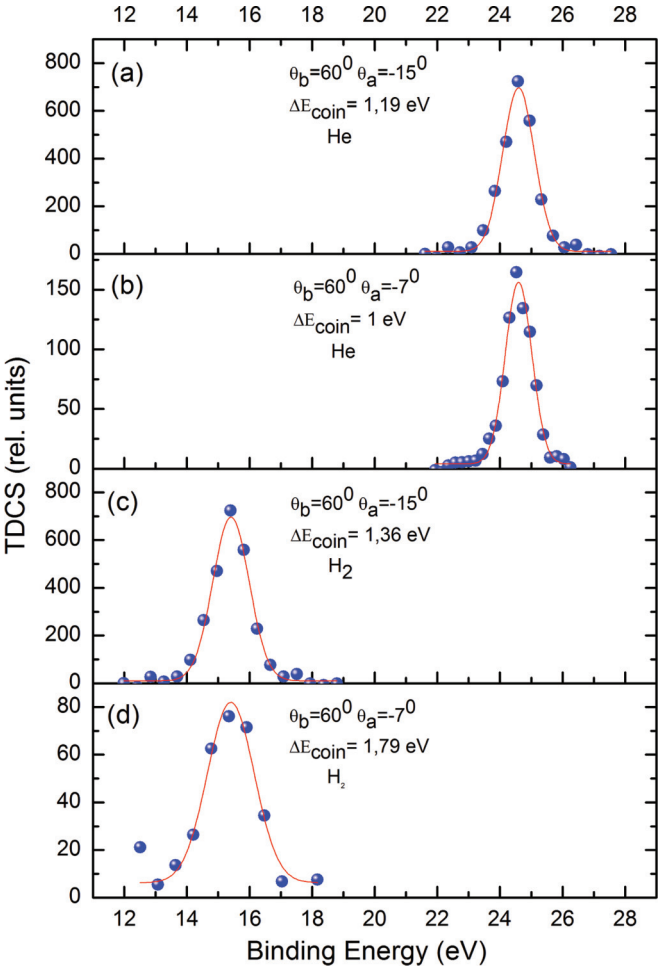

FIG. 3. (Color online) Binding energy spectra for He and H_2. The kinematics are $E_0 = 250$ eV and $E_b = 50$ eV. Panels (a) and (b) show He binding energy spectra for projectile scattering angles of -15° and -7°. Panels (c) and (d) show the binding energy spectra for H_2 also for projectile scattering angles of -15° and -7°.

contributions is the coincidence peak for the fully correlated events. Figure 3 presents the binding energy spectra that show the coincidence count rates as a function of scattered electron energy for He and H_2 targets. The H_2 binding energy spectrum is broader than the He spectrum, as was also seen in Refs. [15,16]. The ejected electron energy is 50 eV for both cases. Binding energy spectrum were recorded for each energy and projectile scattering angle.

III. THEORETICAL FRAMEWORK

The most sophisticated current theories for the electron-impact molecular ionization process are the first Born approximation in which the two-center continuum wave approximation with correct boundary conditions is applied in both the incident and exit channels [23], the molecular three-body distorted wave approximation (M3DW) coupled with an orientation-averaged molecular orbital approximation [24], and the time-dependent close coupling (TDCC) approximation [25]. Al-Hagan *et al.* [26] showed that the M3DW method yielded good agreement with experimental TDCS data for H_2, and this is the theoretical approach we will use here.

The molecular three-body distorted wave (M3DW) approximation has been presented in previous publications [27–29], so only the main points of the theory will be presented. The TDCS for the M3DW is given by

$$\frac{d\sigma}{d\Omega_a d\Omega_b dE_b} = \frac{1}{(2\pi)^5}\frac{k_a k_b}{k_i}(|T_{\rm dir}|^2 + |T_{\rm exc}|^2 + |T_{\rm dir} - T_{\rm exc}|^2), \tag{3}$$

where $\vec{k}_i$, $\vec{k}_a$, and $\vec{k}_b$ are the wave vectors for the initial, scattered, and ejected electrons, $T_{\rm dir}$ is the direct scattering amplitude, and $T_{\rm exc}$ is the exchange amplitude. The direct scattering amplitude is given by

$$T_{\rm dir} = \langle \chi_a^-(\vec{k}_a,\mathbf{r}_1)\chi_b^-(\vec{k}_b,\mathbf{r}_2)C_{\rm scat-eject}(r_{12}^{av}) \times |V - U_i|\phi_{DY}^{OA}(\mathbf{r}_2)\chi_i^+(\vec{k}_i,\mathbf{r}_1)\rangle, \tag{4}$$

where $\mathbf{r}_1$ and $\mathbf{r}_2$ are the coordinates of the incident and the bound electrons, χ_i, χ_a, and χ_b are the distorted waves for the incident, scattered, and ejected electrons, respectively, and $\phi_{DY}^{OA}(r_2)$ is the initial bound-state Dyson molecular orbital averaged over all orientations. The factor $C_{\rm scat-eject}(r_{12}^{av})$ is the Ward-Macek average Coulomb-distortion factor between the two final-state electrons [30], V is the initial-state interaction potential between the incident electron and the neutral molecule, and U_i is a spherically symmetric distorting potential which is used to calculate the initial-state distorted wave for the incident electron $\chi_i^+(\vec{k}_i,\mathbf{r}_1)$. For the exchange amplitude $T_{\rm exc}$, particles 1 and 2 are interchanged in Eq. (4).

The Schrödinger equation for the incoming electron wave function is given by

$$\left(T + U_i - \frac{k_i^2}{2}\right)\chi_i^+(\vec{k}_i,\mathbf{r}) = 0, \tag{5}$$

where T is the kinetic energy operator and the $+$ superscript on $\chi_i^+(\vec{k}_i,\mathbf{r})$ indicates outgoing-wave boundary conditions. The initial-state distorting potential contains three components $U_i = U_s + U_E + U_{CP}$, where U_s contains the nuclear contribution plus a spherically symmetric approximation for the interaction between the projectile electron and the target electrons, which is obtained from the quantum-mechanical charge density of the target. The charge density is $2|\phi_{DY}|^2$ (the 2 is for double occupancy and the original nonaveraged Dyson orbital is used). The nuclear contribution to U_s is the interaction between the projectile electron and the two nuclei averaged over all orientations. Averaging the nuclei over all orientations is equivalent to putting the nuclear charge of 2 on a thin spherical shell whose radius is the distance of the nuclei from the center of mass (c.m.) (0.7 a_0).

U_E is the exchange potential of Furness-McCarthy (corrected for sign errors) [31], which approximates the effect of the continuum electron exchanging with the passive bound electrons in the molecule, and U_{CP} is the correlation-polarization potential of Perdew and Zunger [32] (see also Padial and Norcross [33]).

In Eq. (4), the final state for the system is approximated as a product of distorted waves for the two continuum electrons (χ_a^-, χ_b^-) times the Ward-Macek average Coulomb-distortion factor $C_{\rm scat-eject}$. The final-state distorted waves are calculated the same as the initial state except that the final-state charge density is used to calculate U_s. The final-state charge density is

obtained the same as the initial state except that the occupancy number is unity. Additional details can be found in Madison and Al-Hagan [24].

IV. RESULTS AND DISCUSSION

Figures 4 and 5 compare the experimental and theoretical TDCS for 250-eV electron-impact ionization of He and H_2. On each figure, the left-hand column is the energy scan for a fixed projectile scattering angle of 15° and the right-hand column is a scattered projectile angular scan for a fixed ejected electron energy of 50 eV. The typical binary peaks for small ejection angles and recoil peaks for large ejection angles are evident from the figures (although the recoil peaks tend to be very small for these kinematics). The theoretical and experimental results are normalized to unity at the binary peak. The solid circles are the present results and the stars are the results of Milne-Brownlie *et al.* [15]. It is seen that the present experimental results are in very good agreement with those of Milne-Brownlie *et al.* [15], with the possible exception of the He recoil peak for 15 eV. However, the Milne-Brownlie *et al.* [15] measurements were made for 10 eV, which is

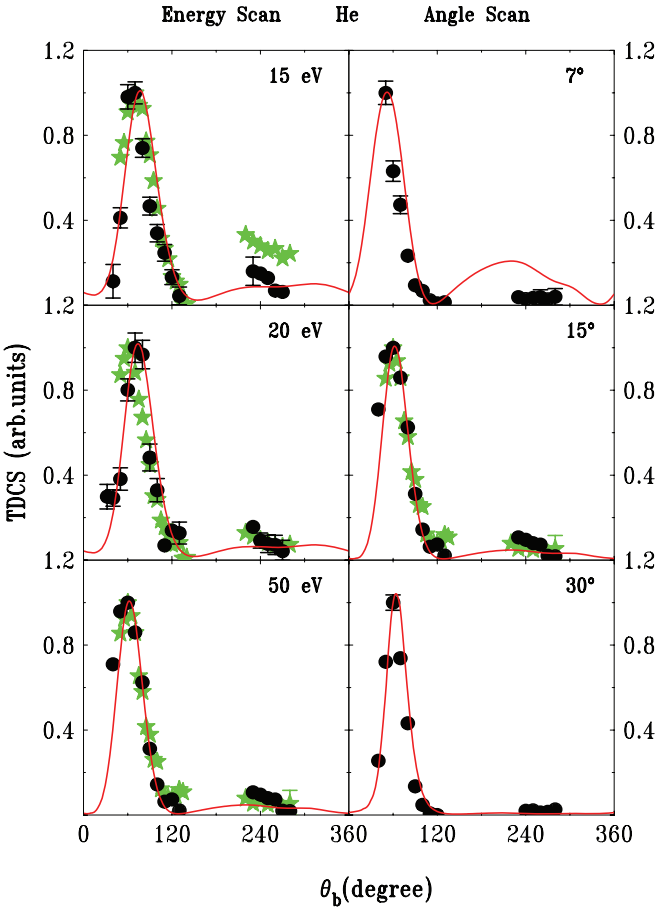

FIG. 4. (Color online) TDCS for 250-eV electron-impact ionization of He as a function of the ejected electron angle θ_b. For the left-hand column, the projectile scattering angle is $\theta_a = 15^\circ$ and the energy of the ejected electron is noted. For the right-hand column, the ejected electron energy is 50 eV and the projectile scattering angle is noted. Solid circles– present data, stars– data of Milne-Brownlie *et al.* [15], and solid (red) curve– 3DW.

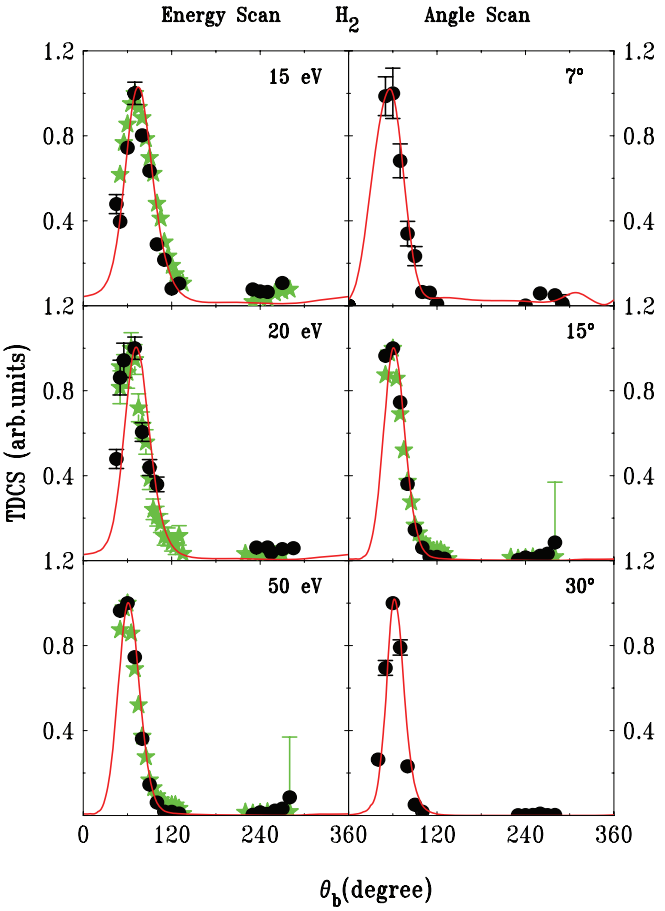

FIG. 5. (Color online) Same as Fig. 4 except for ionization of H_2.

inaccessible for us, so we have plotted their 10-eV results with our 15-eV results.

It is seen that overall there is also very good agreement between experiment and theory. The only significant disagreement between experiment and theory is seen for the He recoil peak for 7° in the angular scan. The disagreement with the Milne-Brownlie *et al.* [15] recoil peak for He 15 eV in the energy scan is not due to the energy difference mentioned above. We calculated M3DW TDCS for 10-eV ejected electron energy (same as the data) and our theoretical results are noticeably smaller than the Milne-Brownlie *et al.* [15] recoil peak and closer to the present 15-eV recoil peak. We would also note that there is a small difference between the two experiments for the 20-eV He binary peak position and the theoretical results are in excellent agreement with the present measurements.

Looking only at the TDCS angular distributions, one cannot see anything remarkably different between the energy scan and angular scan. To see the possible effects of Young's-type interference, we need to look at the ratio of the molecular cross section to the atomic cross section to get the interference factor I. Figure 6 shows the theoretical and experimental I factors for the energy and angular scans (using He for the denominator). We have arbitrarily normalized theory to unity at one of the peaks and experiment to the best visual fit to theory. Also shown is the Cohen-Fano I^{CF} of Eq. (1) (dashed blue curve).

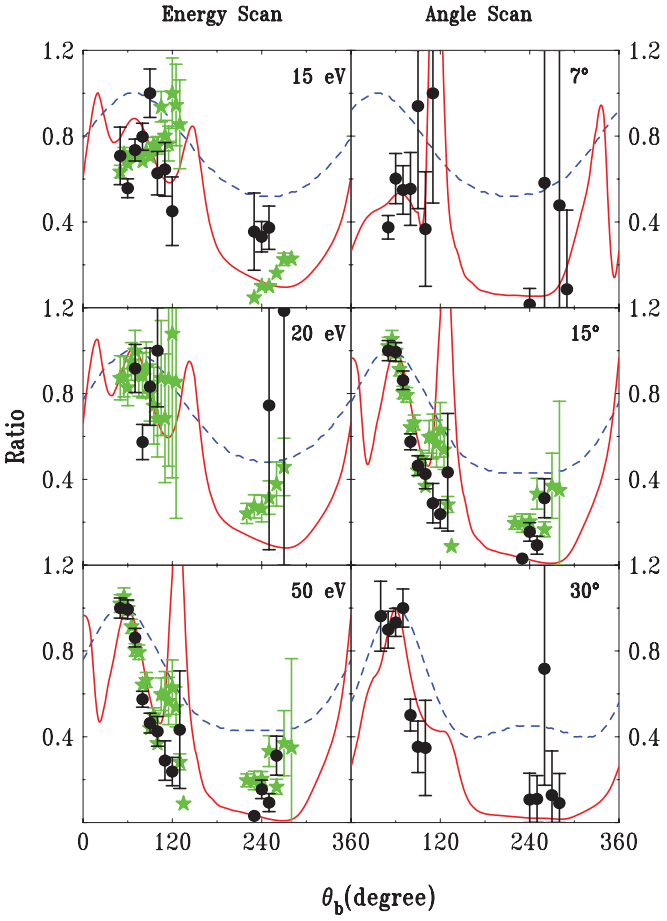

FIG. 6. (Color online) Interference factor for 250-eV electron-impact ionization of H_2 and He as a function of the ejected electron angle θ_b. For the left-hand column, the projectile scattering angle is $\theta_a = 15^\circ$ and the energy of the ejected electron is noted. For the right-hand column, the ejected electron energy is 50 eV and the projectile scattering angle is noted. Solid circles– present data, stars– data of Milne-Brownlie *et al.* [15], solid (red) curve– M3DW, and dashed (blue) curve– I^{CF}.

Overall, there is a qualitative agreement with I^{CF}. As mentioned above, Casagrande *et al.* [16] presented these same ratios for higher electron energies (~600 eV) and they found good agreement with the shape of the I^{CF} factor in their energy scan results. However, from Fig. 6 it is seen that both experiment and theory exhibit a much more complicated structure, particularly for the binary region for the present kinematics. In general, there is very good agreement between the M3DW I factor and experiment.

In the energy scan, the M3DW I factors have a triple-peak structure for the binary region. Although the first peak is in an angular range inaccessible to experiment, the other two peaks lie mostly in the measured angular range. For the two lower energies, there is sufficient scatter in the data so that all one can say is that the data is consistent with the possibility of two peaks. However, for the 50-eV case, it is clear that the experiment also has two peaks, although the second experimental peak appears to be smaller than the predicted theoretical one. For the recoil peak angular range, both the experiment and the M3DW predict a greater suppression relative to the binary peak than that predicted by the I^{CF} factor.

Comparing the I factors for the energy scan and angular scan, it is seen that the I factor changes more dramatically with changing angle than with changing energy. For the energy scan, there are three peaks in the binary region for all three cases and, with increasing energy, the only noticeable changes are relative peak heights and a small change in peak location. For the angle scan, on the other hand, the M3DW I factor has two peaks at 7°, three peaks at 15°, and only a single peak with a shoulder at 30°, and the experimental data exhibit this same structure!

Previously, the observation of a suppressed recoil peak for molecular H_2 was thought to be sufficient evidence indicating Young's-type interference [15]. Here we see a much larger and more interesting consequence of interference, with significant structure in the binary region which has not been seen before. The important question concerns the physical effects which cause this structure. Obviously, there are going to be a lot of different types of interference effects contributing to any quantum-mechanical calculation. Presumably, taking the ratio of the molecular to atomic cross sections isolates the molecular double-slit effects. However, the I^{CF} factor attributed to the

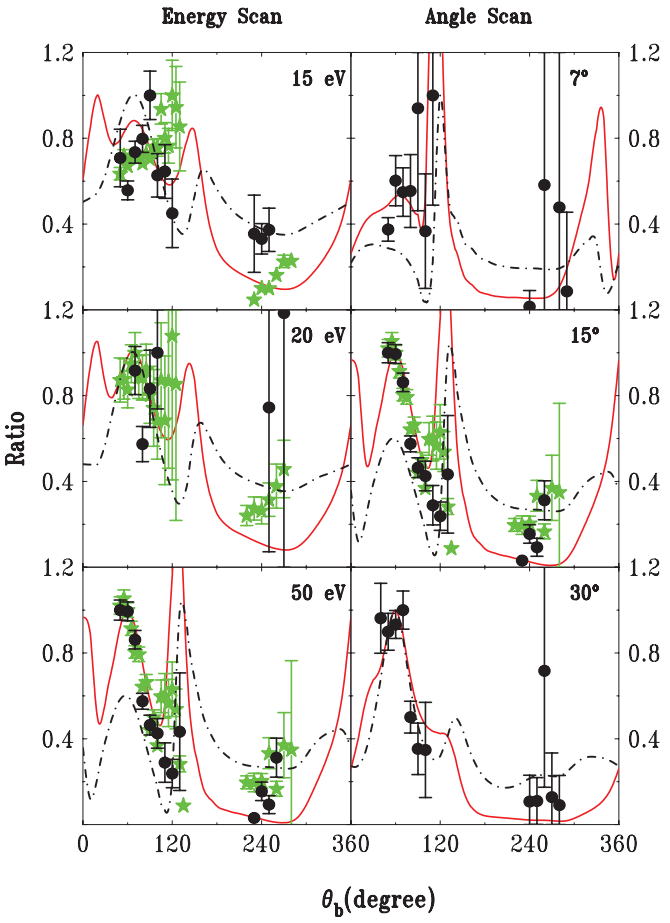

FIG. 7. (Color online) Same as Fig. 6 except that the solid (red) curve is the full M3DW calculation, and the dot-dash (black) curve is the model calculation with the only molecular contribution being the diffraction of the incident projectile from two scattering centers.

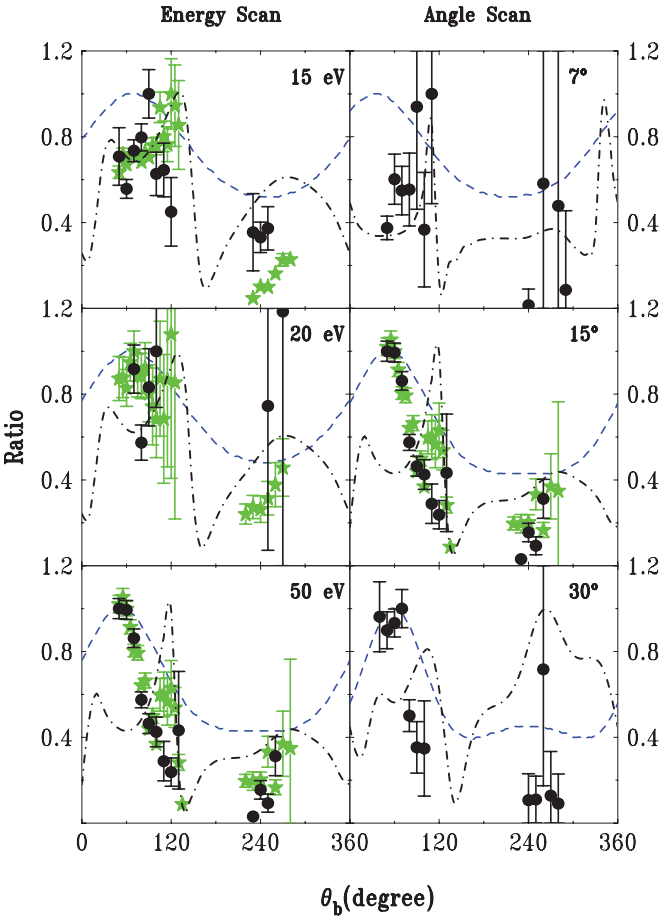

FIG. 8. (Color online) Same as Fig. 6 except that the dashed-dot curve is the model calculation with the only molecular contribution being the emission of the ejected electron from two scattering centers and the dashed (blue) curve is I^{CF}.

ejected electron being emitted from two nuclear centers is just one of the possible molecular double-slit interference effects. A second possible interference effect is the diffraction of the incoming projectile from two scattering centers, and a third possibility is the motion of the scattered projectile in the field of two scattering centers.

One of the big advantages of the present perturbation approach lies in the fact that different physical effects like this can be isolated in the calculation. For example, the effect of the ejected electron being emitted from two scattering centers can be modeled by performing a helium calculation, except replace the ejected electron distorted wave $\chi_b^-(\vec{k}_b,\mathbf{r}_2)$ calculated using a helium-ion potential with a H_2 distorted wave calculated using the H_2-ion potential. Likewise, the effect of the scattered projectile being emitted from two scattering centers can be modeled by performing a helium calculation, except replace the scattered electron distorted wave $\chi_a^-(\vec{k}_a,\mathbf{r}_1)$ calculated using a helium-ion potential with a H_2 distorted wave calculated using the H_2-ion potential. Finally, the effect of the incident electron diffracting from two scattering centers can be modeled by performing a helium calculation, except replace the initial channel helium wave functions with molecular wave functions (i.e., molecular bound-state wave function and the incident channel distorted wave calculated using the neutral molecular distorting potential).

We have performed these three different model calculations and the results clearly demonstrate that the most important process is the diffraction of the incident electron from two scattering centers. In Fig. 7, the I factor is presented for the full molecule calculation (solid red curve) and the model calculation treating only the initial state as a molecule (dot-dashed black curve). It is seen that the two calculations yield very similar I factors, which means that most of the double-slit interference effects contributing to the structure in the I factor are contained in the diffraction of the incoming projectile from two scattering centers.

It is also interesting to compare the I factor by treating just the ejected electron as a molecular wave with I^{CF}, since they are presumably modeling the same physical effects. This comparison is contained in Fig. 8, where it is seen that the two calculations yield very different results. Although I^{CF} was valid for 600-eV electrons [16], it is clearly not a good approximation for the present energies.

V. CONCLUSION

This paper presents experimental and theoretical results for 250-eV electron-impact ionization of He and H_2. Results were presented for (1) an ejected electron energy scan of 15, 20, and 50 eV for a fixed projectile scattering angle of 15° and for (2) a projectile angular scan of 7°, 15°, and 30° for a fixed ejected electron energy of 50 eV.

We have examined the I factor and we found that the I factor has significantly more structure than I^{CF} and that it is more sensitive to the angle scan than to the energy scan. The Cohen-Fano model where the two atoms in the molecule are independent absorbers of energy which then became two separate sources for the emission of electrons was previously believed to accurately describe Young's-type interference effects for electron-impact TDCS of diatomic molecules. Here we see that while there is an overall qualitative agreement with I^{CF}, both experiment and theory predict a much more complicated interference pattern in the binary peak region.

We separately examined the three different types of contributions to the microscopic double-slit interference pattern and found that the most important contribution comes from the incident projectile diffracting from two scattering centers. We also compared the contribution of the ejected electron being emitted from two scattering centers with I^{CF}, which presumably contains the same physical effects, and found that the results were very different, indicating that I^{CF} is not a good approximation for the kinematics considered here.

Obviously, any quantum-mechanical calculation can and will have multiple different types of interference effects contributing to the final results. The main idea of the I factor introduced by Cohen-Fano is that all of the non–two-center interference effects can be eliminated by dividing by the atomic cross section. Here, as in previous works, we have divided by atomic He cross sections instead of atomic H cross sections. Obviously, the practical problem is that experimental

atomic H cross sections are very hard to measure. For several of the heavy-particle DDCS measurements referenced here [2–5,9,10], theoretical atomic H cross sections were used and that work has been criticized as not representing a clean comparison between experiment and theory. Using He allows for a clean comparison between experiment and theory. Helium is also appealing since it has the same number of electrons and protons as H_2. The only downside is that one cannot be sure that all of the non–two-center interference effects will have been divided out. Even if this is not the case, the comparison with theory is still valid. What will not be valid is our assumption that the observed structure results only from the three different types of possible two-center interference effects which we have identified. In Fig. 7, the solid (red) curve represents all the interference structure not contained in He (whether it be two-center or not). The dashed-dot curve represents the effect of the incident projectile diffracting from two scattering centers. The similarity of these two curves would indicate that most, if not all, of the structure seen in the solid (red) curve stems from two-center effects.

ACKNOWLEDGMENTS

This work was supported by the Scientific and Technological Research Council of Turkey (TUBITAK) through Grant No. 109T738. The theoretical work of H.C. and D.M. was supported by the US National Science Foundation under Grant. No. PHY-1068237.

[1] H. D. Cohen and U. Fano, Phys. Rev. **150**, 30 (1966).
[2] N. Stolterfoht, B. Sulik, V. Hoffmann, B. Skogvall, J. Y. Chesnel, J. Rangama, F. Fremont, D. Hennecart, A. Cassimi, X. Husson, A. L. Landers, J. A. Tanis, M. E. Galassi, and R. D. Rivarola, Phys. Rev. Lett. **87**, 023201 (2001).
[3] N. Stolterfoht *et al.*, Phys. Rev. A **67**, 030702(R) (2003).
[4] S. Hossain, A. L. Landers, N. Stolterfoht, and J. A. Tanis, Phys. Rev. A **72**, 010701 (2005).
[5] D. Misra, U. Kadhane, Y. P. Singh, L. C. Tribedi, P. D. Fainstein, and P. Richard, Phys. Rev. Lett. **92**, 153201 (2004).
[6] C. Dimopoulou *et al.*, Phys. Rev. Lett. **93**, 123203 (2004).
[7] O. Kamalou, J. Y. Chesnel, D. Martina, F. Fremont, J. Hanssen, C. R. Stia, O. A. Fojon, and R. D. Rivarola, Phys. Rev. A **71**, 010702(R) (2005).
[8] D. Misra, A. Kelkar, U. Kadhane, A. Kumar, L. C. Tribedi, and P. D. Fainstein, Phys. Rev. A **74**, 060701(R) (2006).
[9] J. A. Tanis, J. Y. Chesnel, B. Sulik, B. Skogvall, P. Sobocinski, A. Cassimi, J. P. Grandin, L. Adoui, D. Hennecart, and N. Stolterfoht, Phys. Rev. A **74**, 022707 (2006).
[10] J. S. Alexander, A. C. Laforge, A. Hasan, Z. S. Machavariani, M. F. Ciappina, R. D. Rivarola, D. H. Madison, and M. Schulz, Phys. Rev. A **78**, 060701(R) (2008).
[11] K. N. Egodapitiya, S. Sharma, A. Hasan, A. C. Laforge, D. H. Madison, R. Moshammer, and M. Schulz, Phys. Rev. Lett. **106**, 153202 (2011).
[12] S. Sharma, A. Hasan, K. N. Egodapitiya, T. P. Arthanayaka, G. Sakhelashvili, and M. Schulz, Phys. Rev. A **86**, 022706 (2012).
[13] A. J. Murray, M. J. Hussey, C. Kaiser, J. Gao, J. L. Peacher, and D. H. Madison, J. Electron Spectrosc. Relat. Phenom. **161**, 11 (2007).
[14] C. R. Stia, A. O. Fojon, P. F. Weck, J. Hanssen, and R. Rivarola, J. Phys. B **36**, L257 (2003).
[15] D. S. Milne-Brownlie, M. Foster, J. Gao, B. Lohmann, and D. H. Madison, Phys. Rev. Lett. **96**, 233201 (2006).
[16] E. M. Casagrande, A. Lahmam-Bennani, and D. H. Madison, J. Phys. B **41**, 025204 (2008).
[17] M. Dogan and A. Crowe, J. Phys. B **33**, L461 (2000).
[18] M. Dogan and A. Crowe, J. Phys. B **35**, 2773 (2002).
[19] M. Stevenson and A. Crowe, J. Phys. B **37**, 2493 (2004).
[20] M. Dogan, A. Crowe, K. Bartschat, and P. J. Marchalant, J. Phys. B **31**, 1611 (1998).
[21] O. Sise, M. Dogan, I. Okur, and A. Crowe, Phys. Rev. A **84**, 022705 (2011).
[22] M. Dogan, M. Ulu, and O. Sise, J. Electron Spectrosc. Relat. Phenom. **161**, 58 (2007).
[23] C. R. Stia, O. A. Fojon, P. F. Weck, J. Hanssen, B. Joulakian, and R. D. Rivarola, Phys. Rev. A **66**, 052709 (2002).
[24] D. H. Madison and O. Al-Hagan, J. At., Mol., Opt. Phys. **2010**, 367180 (2010).
[25] J. Colgan, M. S. Pindzola, F. Robicheaux, C. Kaiser, A. J. Murray, and D. H. Madison, Phys. Rev. Lett. **101**, 233201 (2008).
[26] O. Al-Hagan, C. Kaiser, D. Madison, and A. Murray, Nat. Phys. **5**, 59 (2009).
[27] J. Gao, D. H. Madison, and J. L. Peacher, J. Chem. Phys. **123**, 204314 (2005).
[28] J. Gao, D. H. Madison, and J. L. Peacher, Phys. Rev. A **72**, 032721 (2005).
[29] J. Gao, D. H. Madison, and J. L. Peacher, J. Chem. Phys. **123**, 204302 (2005).
[30] S. J. Ward and J. H. Macek, Phys. Rev. A **49**, 1049 (1994).
[31] J. B. Furness and I. E. McCarthy, J. Phys. B **6**, 2280 (1973).
[32] J. P. Perdew and A. Zunger, Phys. Rev. B **23**, 5048 (1981).
[33] N. T. Padial and D. W. Norcross, Phys. Rev. A **29**, 1742 (1984).